

# Stability and Degradation of Metal–Organic-Framework Films under Ambient Air Explored by Uptake and Diffusion Experiments

Chun Li, Abhinav Chandresh, Zejun Zhang, Sarah Moulai, and Lars Heinke\*

The loading with guest molecules is the key feature for most applications of metal–organic frameworks (MOFs). The limited stability of MOFs against environmental factors, like humid air, is often a severe problem which hinders real-life applications. Here, the stability of four common MOFs, UiO-66, UiO-67, HKUST-1, and ZIF-8, under long-term exposure to humid air and under exposure to water vapor is explored. Transient uptake experiments with toluene and other volatile organic compounds as probe molecules are combined with structural investigations via X-ray diffraction and infrared spectroscopy. In line with previous publications showing the structural stability of ZIF-8 and UiO-66, it is found that its uptake properties are not affected by exposure to air. On the other hand, HKUST-1 shows clear structural decomposition in air and degradation of the uptake properties. Unexpectedly, while the diffraction and spectroscopy data of UiO-67 do not suggest a corrosion of the structure upon air exposure, the guest-loading data show a strong decrease of the uptake amount and a deceleration of the uptake rate. Both features strongly indicate the formation of surface barriers for the mass transfer in UiO-67, like in HKUST-1. The study underlines the importance of transient uptake experiments for characterizing the stability of MOF materials.

be tuned over a wide range using appropriate building blocks.<sup>[6]</sup> The MOF properties can be further adjusted by introducing functional groups into the structure or by post synthesis modification.<sup>[7–8]</sup>

Although several chemically robust and water stable MOFs have been presented to date,<sup>[9–10]</sup> a severe drawback of many MOF structure is its limited stability, especially toward exposure to water. Since water vapor is often present in various industrial processes, it must be taken into account when selecting MOF adsorbents and the limited water-stability is a hindering factor for many applications.<sup>[11–12]</sup> In previous works, it was shown that water vapor can corrode the MOF surface, hindering the guest molecule transport through the MOF pores, also known as surface barrier for mass transfer. The existence of surface barriers greatly hinders the application and development of MOFs.<sup>[13–15]</sup>


Here, we explore the mass transfer of a probe molecule (toluene) in MOF films of four popular structures: HKUST-1,

ZIF-8, UiO-66, and UiO-67. HKUST stands for Hong Kong University of Science and Technology, ZIF for zeolitic imidazolate framework and UiO for Universitetet i Oslo. The guest adsorption and diffusion are quantified by using a quartz crystal microbalance (QCM). The MOF films are exposed to common ambient air and the effect on the uptake properties are characterized. While the crystallinities of all MOF films are stable, as shown by X-ray diffraction (XRD), we show that the adsorption amounts and rate constants of toluene in HKUST-1 and UiO-67 severely decrease upon exposure to ambient air. On the other hand, UiO-66 and ZIF-8 are stable and the adsorption and diffusion performance is not affected by long-term contact of the sample with lab air. For unveiling the defects and clarifying the degradation mechanism, we use infrared spectroscopy and can correlate the defects causing the increased mass transfer resistance with previously described defects. For UiO-67, the experiments are complemented with uptake experiments with different guest molecules as well as with a MOF powder, showing a similar degradation and evolution of surface barriers. Such surface barriers for the mass transfer, as found in UiO-67 MOFs, have not yet been reported for UiO-type MOFs. The study shows that although the crystallinity of the material

## 1. Introduction

Nanoporous modular framework materials attract substantial attention due to their wide variety and unique properties, such as large surface area and high gas storage capacity.<sup>[1–4]</sup> In particular, metal–organic frameworks (MOFs) are explored intensively. MOFs are self-assembled from metal nodes connected by organic di- or multi-topic linker molecules.<sup>[5]</sup> The properties of MOF can

C. Li, A. Chandresh, Z. Zhang, S. Moulai, L. Heinke  
Karlsruhe Institute of Technology (KIT)  
Institute of Functional Interfaces (IFG)  
Hermann-von-Helmholtz-Platz 1,  
76344 Eggenstein-Leopoldshafen, Germany  
E-mail: Lars.Heinke@KIT.edu

 The ORCID identification number(s) for the author(s) of this article can be found under <https://doi.org/10.1002/admi.202101947>.

© 2021 The Authors. Advanced Materials Interfaces published by Wiley-VCH GmbH. This is an open access article under the terms of the Creative Commons Attribution-NonCommercial License, which permits use, distribution and reproduction in any medium, provided the original work is properly cited and is not used for commercial purposes.

DOI: 10.1002/admi.202101947

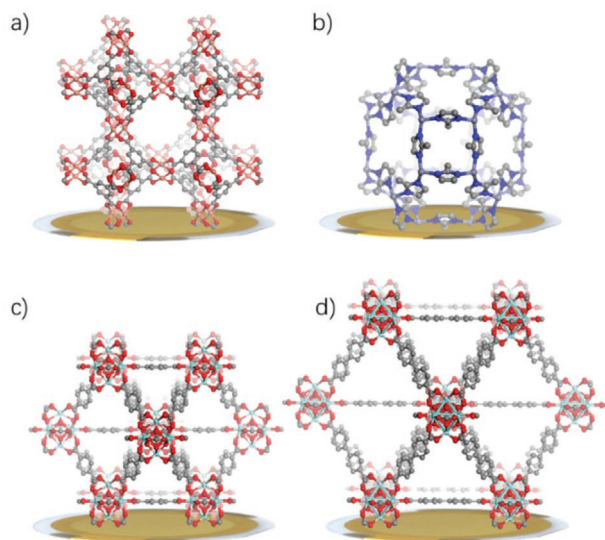


**Figure 1.** Investigated MOF structures: a) HKUST-1, b) ZIF-8, c) UiO-66, and d) UiO-67.

is essentially unaffected, the uptake properties, which are essential for most applications, need to be explored in detail.

## 2. Results and Discussion

### 2.1. Characterization of MOF Films

Four different representatives of MOF films with structure of type HKUST-1, UiO-66, UiO-67, and ZIF-8 were selected because they are among the most popular and most thoroughly explored MOF structures. They find use in many applications.<sup>[9–10,13]</sup>

HKUST-1 is built from copper-dimers connected by benzene-1,3,5-tricarboxylate (BTC) molecules, see **Figure 1a**; **Figure S1a** in the Supporting Information. The structures of UiO-66 and UiO-67 are shown in **Figure 1c,d**. UiO-type MOF has been reported to possess exceptional stability,<sup>[16]</sup> which is attributed to the cuboctahedra metal node ( $Zr_6O_4(OH)_4$ ) allowing for the coordination of 12 BDC or BPDC linker molecules (**Figure S1c,d**, Supporting Information). ZIF-8 also has a 3D framework, however, very different from the above-mentioned MOFs.<sup>[9]</sup> In its structure, the ligands are directly bonded to the metal via Zn–N coordination (**Figure 1b**; **Figure S1b**, Supporting Information), not via metal–carboxylate bonds.

The MOF films were prepared by layer-by-layer (lbl) SURMOF syntheses in the case for HKUST-1 and ZIF-8 and by vapor-assisted conversion (VAC) MOF film synthesis for UiO-66 and UiO-67. More details can be found in the Experimental Section. In all cases, the MOF films are grown directly on the substrates, which are functionalized gold-coated QCM sensors.

The morphology and thickness of the MOF films were characterized by scanning electron microscopy (SEM), **Figure 2**. All four MOF films have an essentially homogenous morphology where the films are composed of crystallites of about 0.1 to 0.4  $\mu\text{m}$  extension. The octahedral morphology of many crystallites as well as many triangular crystal facets are visible. The thicknesses of the HKUST-1, UiO-66, UiO-67, and ZIF-8

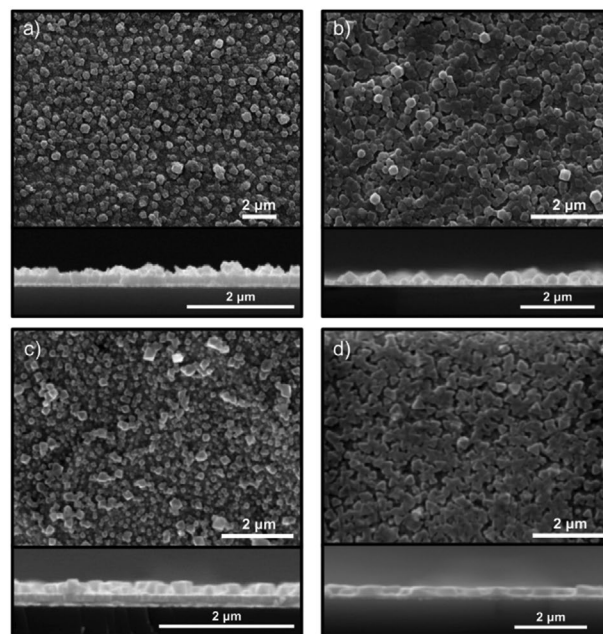


**Figure 2.** SEM images of a) HKUST-1, b) ZIF-8, c) UiO-66, and d) UiO-67. The upper parts of the panels show the top view of the MOF thin films. The lower parts show the cross sections of the broken samples.

MOF films are similar and were estimated to  $\approx 0.2 \pm 0.1 \mu\text{m}$ , see **Figure 2**.

The crystallinities of the samples were explored by XRD. The X-ray diffractograms of all samples verify that the MOF films have the targeted structures. The formation of HKUST-1 film was confirmed by comparison with the calculated XRD pattern (**Figure 3a**; **Figure S2a**, Supporting Information). Moreover, the XRD data show that the HKUST-1 MOF film is grown in the crystalline (100) orientation perpendicular to the substrate surface. The formation and crystalline MOF growth of UiO-66, UiO-67, and ZIF-8 are also verified by XRD, **Figure 3**; **Figure S2**, Supporting Information.

The crystallinity of the MOF films during the exposure to common air is also shown in **Figure 3**. The crystallinities of UiO-66, UiO-67, and ZIF-8 are essentially constant. This means, a decrease of crystallinity of the MOF material upon exposure to common air cannot be observed for these MOF films. On the other hand, the crystallinity of the HKUST-1 film clearly decreases upon the exposure to air. The intensity of the XRD reflexes decreases by a factor of  $\approx 4$  upon the exposure of the sample to air for 30 days. This is a strong indication for the instability of HKUST-1, as also previously reported in the literature.<sup>[13,17]</sup>

### 2.2. Uptake Experiments with the Samples upon Exposure to Air

The transient uptake by the four MOF films were studied using a QCM. Due to its size, volatility and relatively low health hazard, we chose toluene as the probe molecule. The adsorption and desorption processes of toluene are rather fast, so the uptake or release was finished within a few seconds to minutes upon changing the gas composition. For the pristine sample, the uptake experiments were repeated three times in **Figure S3** in the Supporting Information. The adsorption amount and rate did not change significantly, showing the repeatability and reproducibility of the data.

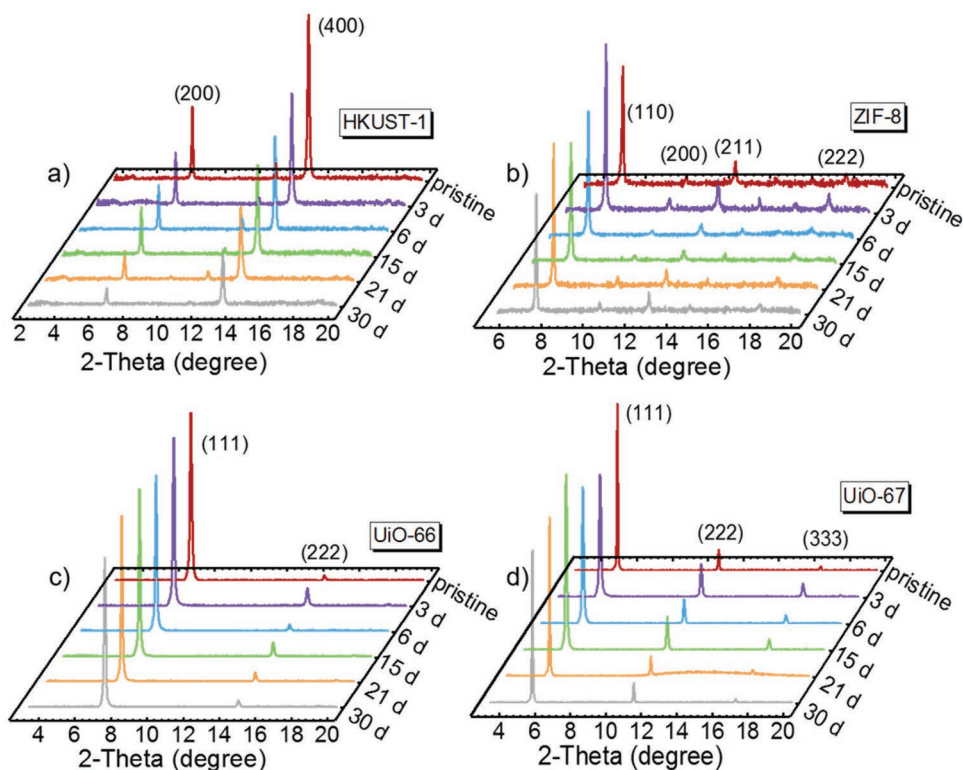


**Figure 3.** XRDs of the MOF films of type a) HKUST-1, b) ZIF-8, c) UiO-66, and d) UiO-67. The observed diffraction peaks are labeled. The exposure times toward air are labeled. The calculated XRD of the MOFs are shown in Figure S2 in the Supporting Information.

The uptake of toluene was recorded for the pristine MOF films. Subsequently, the MOF films are exposed to common (humid) air for a few days and the uptake experiments were then repeated. Typical uptake curves of toluene in the four MOF films are shown in **Figure 4**; Figure S4 in the Supporting Information.

For HKUST-1 (Figure 4a), the exposure to air decreases the toluene uptake amount and decelerates the uptake rates. Both findings are in agreement with previous experiments in HKUST-1, e.g., by using cyclohexane as probe molecules.<sup>[13]</sup> There, the formation of surface barriers was observed, hindering the guest molecules entering or leaving the MOF pore space.<sup>[18–22]</sup>

The uptake of toluene by the ZIF-8 film is shown in Figure 4b. There, the uptake curves are not significantly affected by the exposure of the MOF film to air.

For UiO-66 and UiO-67 MOF films, quite different toluene uptake curves were recorded, Figure 4c,d. While the uptake by UiO-66 is not affected by the exposure of the MOF film to air, the uptake by UiO-67 decreases upon exposing the sample to air.

For a detailed analysis, the equilibrium (final) uptake amounts as well as the uptake rates are determined from the data. The uptake amounts of toluene in the MOFs are shown in **Figure 5a**. For UiO-66 and ZIF-8 MOF films, the guest uptake by the MOF is essentially not affected by the exposure of the MOF film to air. In detail, the adsorption capacities in both MOFs decrease only slightly during the initial exposure to air; this means during the first 3 days the toluene uptake amount decreases by 10%–20%. Subsequently, the uptake amount

is unaffected by the air exposure. On the other hand, the uptake amounts of toluene in the MOF films with UiO-67 and HKUST-1 structures monotonically decrease upon the exposure of the MOF film to air. For HKUST-1, the adsorption capacity decreases by a factor of  $\approx 7$  during the air exposure for 30 days. The adsorption capacity in UiO-67 decreases by a factor of  $\approx 22$ .

The time constants  $\tau$  of a mono-exponential decay function describing the uptake processes are shown in Figure 5b. It can be seen that the uptake rates of toluene in UiO-66 and ZIF-8 are not significantly affected by the air exposure. In contrast, the uptake rates in HKUST-1 and UiO-67 are significantly decreased. The uptake by HKUST-1 slows down by a factor of  $\approx 400$  when the MOF film is exposed to air for 30 days. While the toluene uptake by the pristine HKUST-1 film reached the equilibrium value in less than 0.1 s, the uptake process takes more than 10 s for the sample after 30-day-air-exposure. In UiO-67, the uptake also slows down by two orders of magnitude.

It should be noted that for the uptake by a homogenous film of thickness  $l$  without surface barriers, the time constant  $\tau$  is correlated to the (intracrystalline) transport diffusion coefficient  $D$  by  $\tau = l^2/(3D)$ .<sup>[18]</sup> With the film thicknesses determined by SEM, the diffusion coefficients of toluene in pristine HKUST-1, ZIF-8, UiO-66, and UiO-67 are calculated to be  $2 \times 10^{-13}$ ,  $1 \times 10^{-15}$ ,  $1 \times 10^{-14}$ , and  $7 \times 10^{-14} \text{ m}^2 \text{ s}^{-1}$ , respectively.

An interesting feature is that the diffusion coefficient increases with increasing diameters of the pore windows, which are 0.34 nm for ZIF-8,<sup>[23]</sup> 0.65 nm for UiO-66, 0.9 nm for UiO-67<sup>[16]</sup> and 1.0 nm for HKUST-1. Please note that, although the size of toluene is larger than the pore window of the frozen

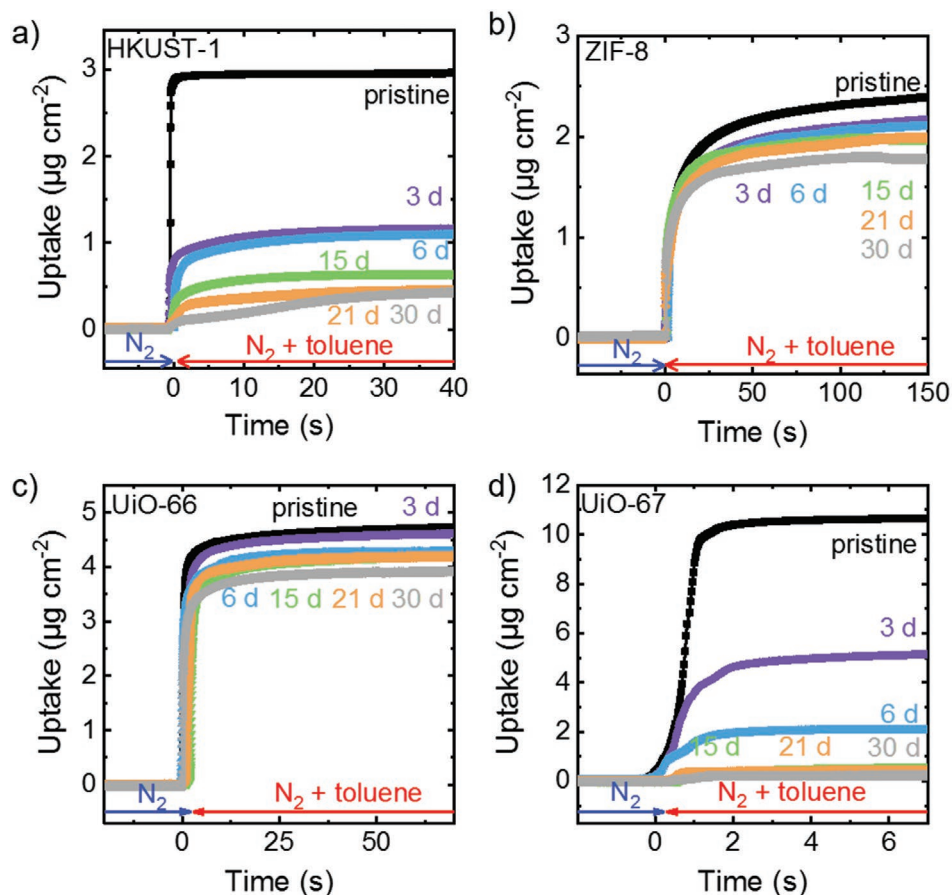


**Figure 4.** Plots of the toluene uptake versus time for a) HKUST-1, b) ZIF-8, c) UiO-66, and d) UiO-67. The exposure times toward air are labeled. The data from a second set of samples are shown in Figure S4 in the Supporting Information.

ZIF-8 structure, the toluene passage through the ZIF-8 pores is enabled by framework flexibility.<sup>[15,24]</sup>

Next, we focus on the MOF films where the air exposure affects the uptake, that is HKUST-1 and UiO-67. The crystallinity of HKUST-1 decreases by a factor of roughly 4 and the UiO-67 crystallinity, as assessed by XRD, does not decline. On the other hand, the uptake amount and rate decrease by one order of magnitude and more. Therefore, we conclude that most MOF material of the film is still intact and crystalline (based on the XRD), but the access for the guest molecules is strongly hindered. This phenomenon is explained by surface defects which causes surface barriers for the mass transfer of the guest molecules. These surface barriers hinder the access to the bulk part of the MOF film and slows down the uptake process.<sup>[18–22,25–27]</sup> In addition, some domains of the MOF material may be fully inaccessible, decreasing the uptake amount. When such defects act as a transport resistance for the molecular uptake in addition to the (intracrystalline) diffusion, the mass transfer is best described by a thin layer at the external MOF surface which has a reduced permeability  $\alpha$ , referred to as surface permeability.<sup>[18]</sup> Then, the time constant for the uptake is given by  $\tau = l^2/(3D) + l/\alpha$ .<sup>[20]</sup> An estimation of the surface permeabilities for the HKUST-1 and UiO-67 MOF films is given in Figure S5 in the Supporting Information. The data show that the surface permeability constantly decreases, this means the

surface barriers for the mass transfer constantly increases, with increasing exposure time of these MOF films to air.

Exposing a pristine UiO-67 sample to water-vapor in pure nitrogen atmosphere shows the same decline of the uptake performance, Figure S6a in the Supporting Information. This indicates that the main reason for the decrease in the adsorption and diffusion performance is caused by water.

To explore whether the observed phenomenon is specific only to toluene, uptake experiments with different guest molecules were performed. To this end, o-xylene, cyclohexane and ethanol were used as probe molecules in addition to toluene. The gas kinetic diameters of the molecules are between 0.4 nm (ethanol) and 0.7 nm (xylene).<sup>[28]</sup> The molar mass varies between 46 g mol<sup>-1</sup> (ethanol) and 106 g mol<sup>-1</sup> (xylene). The uptake by the UiO-67 film, first in the pristine state and then successively degraded in water vapor, are shown in Figure S7 in the Supporting Information. The uptake amounts and the corresponding time constants are shown in Figure 6. The data show clearly that the uptake amount and uptake rate decrease with the water-vapor-exposure of the sample for all studied guest molecules. Thus, the observed phenomenon of surface barriers hindering the molecular uptake is not specific to toluene and is a general phenomenon of the MOF material. A detailed inspection shows that, while the uptake amount changes for all molecules by approximately the same factor, the deceleration of the uptake process of ethanol and

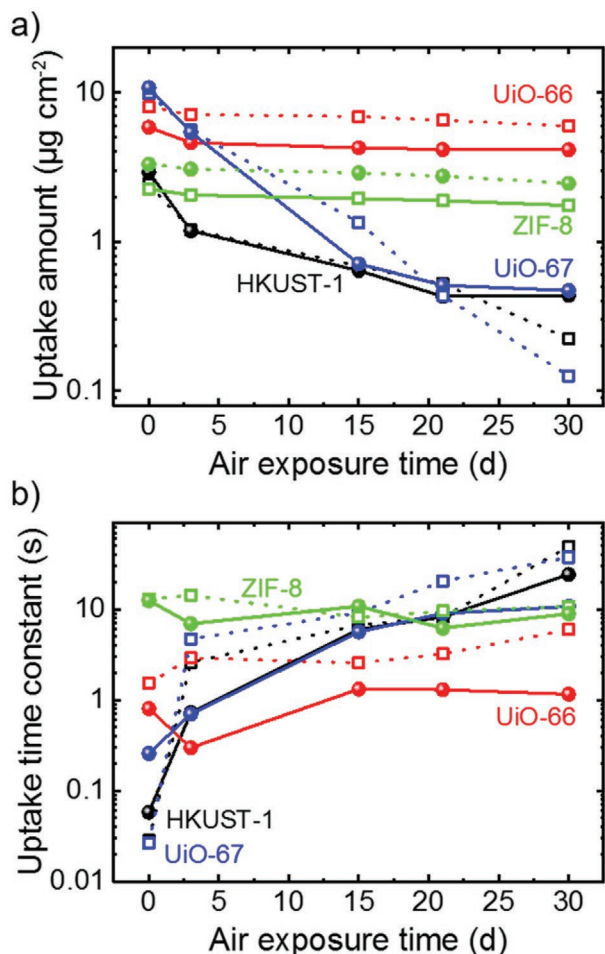


**Figure 5.** a) Amounts and b) time constants for the toluene uptake by the MOF films during the course of the exposure to air for 30 days. The MOF films are shown in black (HKUST-1), green (ZIF-8), red (UiO-66), and blue (UiO-67). The data from two samples for each MOF film, see Figure 4 (filled symbols and solid lines) and Figure S4 in the Supporting Information (open symbols and dotted lines) are shown.

cyclohexane is less pronounced than for o-xylene and toluene. This might be an indication for the nature of the surface barriers in UiO-67, where the large molecules are more hindered than small molecules.

We further explored whether the observed phenomena occur only at MOF films or also at powders. To this end, uptake experiments with different guest molecules and a MOF powder were performed. The XRD and SEM data of the MOF powder are shown in Figure S8 in the Supporting Information. For measuring the uptake by powder in the same sample, the powder was coated on a QCM sensor, see the Experimental Section. The amounts and the corresponding time constants of the guest-molecule uptake by the MOF powder are shown in Figure S9 in the Supporting Information and **Figure 7**. The data clearly show that the uptake process for all molecules also decelerated and the uptake amount decreased upon the exposure of the MOF powder to water vapor. A detailed comparison shows that the effect of the uptake decrease is similar to the MOF film, see Figure 6a versus Figure 7a.

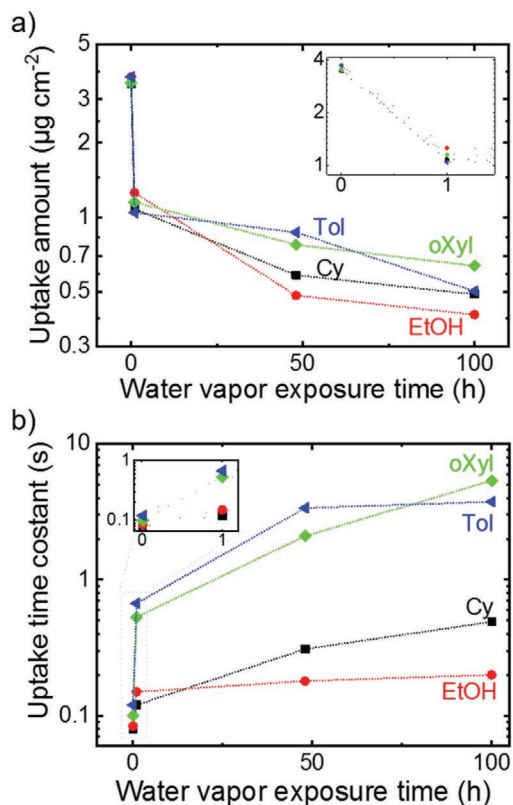


**Figure 6.** a) Amounts and b) time constants for the uptake of different guest molecules by the UiO-67 MOF films during the course of the exposure to water vapor for 100 h. The guest molecules are cyclohexane (Cy, black), ethanol (EtOH, red), o-xylene (oXyl, green), and toluene (Tol, blue). The insets show zoom-ins.

To summarize the QCM uptake experiments, we have compared the effect of ambient air and water-vapor on the degradation of MOF films and a MOF powder and explored the mass transfer. The results indicate that:

- 1) In its pristine state, the toluene uptake by the MOF films is rather fast and the adsorption equilibrium can be reached within less than 1 s, with the exception of ZIF-8, where the uptake takes about 10 s.
- 2) The exposure to air does not affect the guest uptake by ZIF-8 and UiO-66. These MOF films are robust against humidity.
- 3) The uptake capacity and loading rates of HKUST-1 and UiO-67 decreased tremendously upon air exposure. These MOFs are destructed by the humid air or water-vapor, forming surface barriers and thus deteriorating the uptake performance.
- 4) The surface-barrier phenomenon in UiO-67 is not specific to thin films and toluene. It can also be observed in powder samples as well as for different guest molecules.

### 2.3. Vibrational Spectroscopy and Discussion of Degradation

For a better understanding of the defects in the MOF, vibrational infrared reflection absorption (IRRA) spectra were

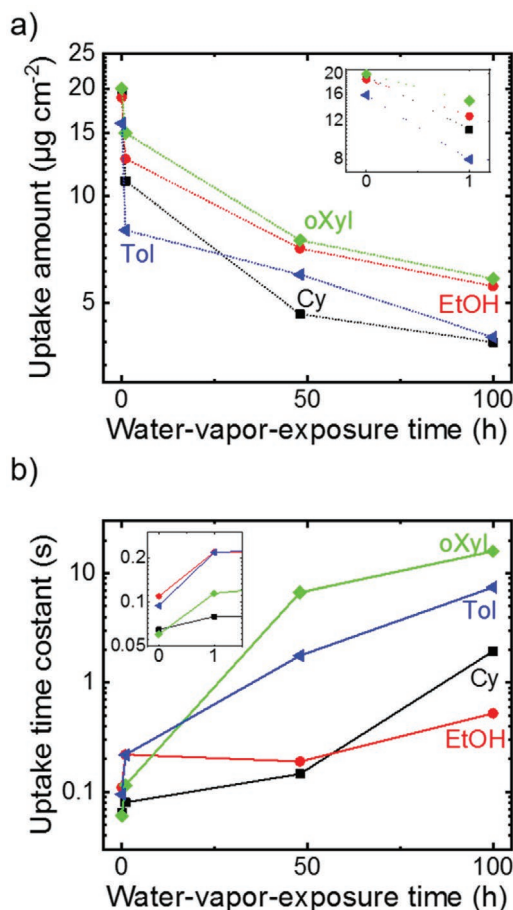


**Figure 7.** a) Amounts and b) time constants for the uptake of different guest molecules by the UiO-67 MOF powder during the course of the exposure to water vapor for 100 h. The guest molecules are cyclohexane (Cy, black), ethanol (EtOH, red), o-xylene (oXyl, green), and toluene (Tol, blue). The insets show zoom-ins.

recorded. The spectra of the MOF films in the pristine form and upon exposure to air for up to 30 days are shown in **Figure 8**.

For HKUST-1, **Figure 8a**, an absorption band at  $1708\text{ cm}^{-1}$  in the spectrum is assigned to the C=O, and the bands at  $1650$ ,  $1450$ , and  $1380\text{ cm}^{-1}$  were attributed to  $\text{COO}^-_{\text{asym}}$ , C-H and  $\text{COO}^-_{\text{sym}}$  vibrations, respectively.<sup>[13]</sup> Changes in the IRRA spectra occur with the gradual appearance of bands at  $1708$  and  $1637\text{ cm}^{-1}$  during the exposure to air. The band at  $1708\text{ cm}^{-1}$  is assigned C=O, indicating that the air exposure results in a transformation of the metal carboxylate to carboxylic acid and the bonding between the BTC linker and the Cu node is broken.<sup>[14]</sup> The vibrational mode of molecular water appears at  $1637\text{ cm}^{-1}$ , indicating that water is present during the HKUST-1 destruction. At the same time, a decrease in the intensity of the  $1650$  and the  $1422\text{ cm}^{-1}$  bands was observed, which indicates the transformation of the HKUST-1 carboxylate groups to their protonated acid analogy. The results are in agreement with IRRAS studies of the destruction of HKUST-1 films in a humid nitrogen atmosphere.<sup>[13]</sup> However, the exposure times here are significantly longer than in previous studies. The slower degradation is presumably caused by the smaller relative humidity.

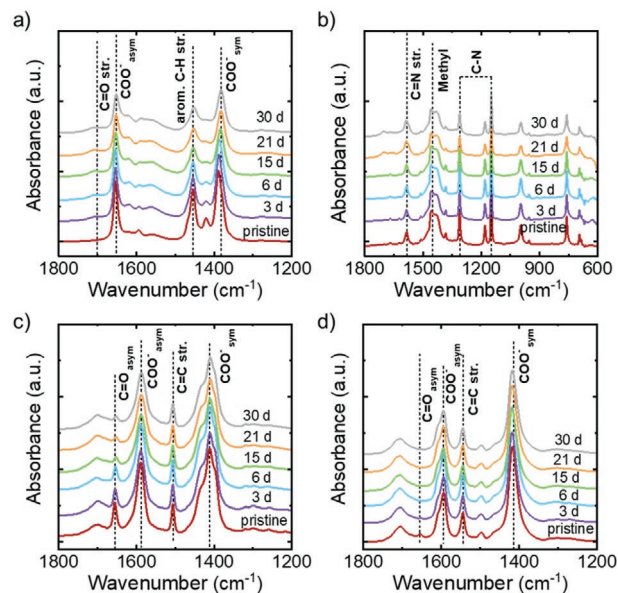


**Figure 8.** IRRA spectra for a) HKUST-1, b) ZIF-8, c) UiO-66, and d) UiO-67. The main vibration bands are labeled. The samples are exposed to humid air for 30 days, see labels.

For ZIF-8, the IRRA spectrum, **Figure 8b**, shows a strong absorption band at  $1587\text{ cm}^{-1}$ , assigned to the C=N stretching.<sup>[15,29–31]</sup> Further intense bands around  $1300$ – $1500\text{ cm}^{-1}$  overlap with the absorption bands of the stretching of imidazole rings.<sup>[32]</sup> The vibration bands are essentially constant and are not affected by exposing the sample to air.

The IRRA spectra of UiO-66 and UiO-67 are shown in **Figure 8c,d**. The vibration bands of the linker and carboxylate groups are labeled. In UiO-66, a small band of DMF (at  $1657\text{ cm}^{-1}$ ) can be seen, which later disappears.<sup>[10,16,33]</sup> A reference experiment, **Figure S10** in the Supporting Information, was performed showing that the DMF band disappears instantly after the activation of the sample at  $65\text{ }^\circ\text{C}$ , as done in the uptake experiments.

It is even more interesting that, although the uptake experiments show a clear performance decrease for UiO-67, only slight decreases were observed in the IRRA spectra at  $1594$ ,  $1544$ , and  $1416\text{ cm}^{-1}$ . For obtaining more insight, IRRA spectra of the same samples under exposure to water vapor is explored, **Figure S6b** in the Supporting Information. A zoom-in of the OCO-symmetric-stretching vibration shows that the band shifts to smaller wavenumbers upon exposing the sample to moisture. This is in line with studies that show the wavenumber decrease of this vibration upon hydroxylation, i.e., breaking the bonding between the linker and the metal node.<sup>[16,34]</sup>

Understanding the breakdown mechanisms in the different MOFs is critical for their applications. The low-stability of HKUST-1 and the high-stability of ZIF-8 toward water and humid exposure was previously reported.<sup>[9,12–13,17,35]</sup> These findings are supported by the uptake, diffraction, and spectroscopy data of the present study. Our data is also in line with the HKUST-1 degradation mechanism suggested in refs [12]. For UiO-66, pronounced stability against humid air and water was found based on XRD and spectroscopy studies.<sup>[10,17]</sup> Our data

verify that the uptake by the MOF materials is also not affected by humidity exposure.

For UiO-67, the situation is more complex. While a number of articles state that UiO-67 is stable against exposure to water,<sup>[16,36–37]</sup> many articles state that UiO-67 degrades under moisture.<sup>[38–42]</sup> Our data show that while the crystallinity and vibrational spectra are barely affected by the water exposure, the uptake performance reduces tremendously. The paradox is resolved by stressing where the respective signals come from: The diffraction and spectroscopic data are dominated by the bulk part of the film and are only slightly affected by the external MOF surface. This means, the destruction of the external MOF surface to an amorphous impermeable layer has barely an effect on the XRD and IR data. On the other hand, such a layer with a large mass transfer resistance reduces the uptake rate and amount tremendously, as observed. This fact stresses the need for precise uptake experiments to characterize the material stability, since the loading and interaction with guest molecules are often the key property of MOFs.

### 3. Conclusions

By uptake experiments using toluene as probe molecules, complemented by X-ray diffraction, vibrational spectroscopy and uptake experiments with different guest molecules, the effect of exposure to common humid air and to water vapor on the stability and uptake performance of four frequently used MOF structures was explored. For ZIF-8 and UiO-66, the structure as well as the guest uptake is unaffected by the exposure of the MOF film to air for many weeks. For HKUST-1, it was found that the MOF material degradation in air is similar to the degradation in humid nitrogen atmosphere, indicating the importance of humidity. For UiO-67, we found that the uptake performance deteriorates upon air exposure or upon water-vapor exposure, similar to HKUST-1, although diffraction and vibrational studies provide no indication for a degradation. The decline of the uptake performance in these two MOFs is explained by the formation of surface barriers, hindering the molecules in entering and leaving the pore space.

With regard to applications where the guest loading is crucial, like catalysis and selective adsorption, the study shows that uptake experiments are fundamental for classifying the stability of a MOF material, while diffraction and spectroscopy data may not be sufficient.

### 4. Experimental Section

**Chemicals:** Copper acetate monohydrate 99.9% ( $\text{Cu}(\text{CH}_3\text{COO})_2 \cdot \text{H}_2\text{O}$ ), zirconium chloride 99.9% ( $\text{ZrCl}_4$ ), zirconyl chloride octahydrate 98% ( $\text{ZrOCl}_2 \cdot 8\text{H}_2\text{O}$ ), and zinc nitrate hexahydrate 98% ( $\text{Zn}(\text{NO}_3)_2 \cdot 6\text{H}_2\text{O}$ ) were purchased from Alfa Aesar; 1,4-benzene dicarboxylic acid 98% (BDC), 1,3,5-benzenedicarboxylic acid 98% (BTC), 4,4-biphenyldicarboxylic acid 98% (BPDC), 2-methylimidazole 99% (MeIm), 11-mercapto-1-undecanol 97% (MUD), 16-mercaptohexadecanoic acid 99% (MHDA), acetic acid 99.8% (HAC), acetone 99.5%, o-xylol 99.8% (oXyl), cyclohexane 99.5% (Cy), toluene 99.8% (Tol), *N,N*-dimethylformamide 99.8% (DMF), and methanol 99.8% (MeOH) from Sigma-Aldrich; ethanol 99.8% (EtOH) and QSense sensors were purchased from VWR and Biolin Scientific, respectively. All chemicals were used without further purification.

**Characterizations:** XRD of the sample was carried out with a Bruker D8 Advance diffractometer equipped with a Si-strip detector (PSD Lynxeye) in  $\theta$ - $\theta$  geometry and a variable divergence slit. The X-ray wavelength is 0.154 nm ( $\text{Cu-K}_{\alpha 1,2}$ ). The diffractograms were recorded over an angular range of  $2\theta = 5.5$ – $20^\circ$ , with a step width of  $2\theta = 0.02^\circ$  and 84 s per step in total.

IRRA spectra measurements were conducted using a Bruker Vertex 80 FTIR spectrometer equipped with a grazing incidence sample accessory providing an angle of  $80^\circ$  relative to the surface normal. A liquid nitrogen-cooled mercury cadmium telluride (MCT) served as the narrow band detector.

**MOF Film Syntheses:** HKUST-1: The HKUST-1 MOF films were synthesized in a layer-by-layer fashion in the QCM cells by alternatively exposing the substrate to the MOF components, i.e., the metal nodes and the linker molecules.<sup>[13]</sup> In detail,  $1 \times 10^{-3}$  M ethanolic copper acetate solution was used as a metal-source and a  $0.2 \times 10^{-3}$  M ethanolic BTC solution as an organic linker source. The synthesis times were: 6 min metal solution, 8 min ethanol, 12 min linker solution, and 8 min ethanol. The flow rate was kept at  $150 \mu\text{L min}^{-1}$ . 50 cycles of HKUST-1 SURMOF films were synthesized. The substrates were gold-coated QCM sensors functionalized with a 16-mercaptohexadecanoic acid (MHDA) self-assembled monolayer (SAM). The HKUST-1 film used in the experiment, which was prepared by the QCM system, had a mass growth curve versus time as shown in Figure S11 in the Supporting Information.

ZIF-8: The synthesis of the ZIF-8 film was performed in a layer-by-layer process using a dipping robot.<sup>[43]</sup> A  $10 \times 10^{-3}$  M zinc dinitrate hexahydrate solution was used as a metal-source and a  $20 \times 10^{-3}$  M 2-methyl-1H-imidazole solution as an organic linker source. The dipping times were as followed: 5 min metal solution, 100 s pure methanol, 5 min linker solution, and 100 s pure methanol. After 200 cycles, the sample was rinsed with ethanol, and dried with  $\text{N}_2$ . The substrates were gold-coated QCM sensors functionalized with 11-mercaptoundecanol (MUD).

UiO-66 and UiO-67: UiO-type MOF films were synthesized via VAC.<sup>[44]</sup> Briefly, the bottom part of a 200 mL Teflon-lined stainless-steel autoclave was filled with Raschig-rings (1 cm  $\times$  1 cm) to obtain an elevated flat platform for the substrate. 4.2 mL DMF and 0.8 mL acetic acid was filled in the autoclave. A QCM sensor was placed on top of the Raschig-rings and fully coated with 40  $\mu\text{L}$  of freshly prepared MOF precursor solution ( $\text{ZrOCl}_2$   $2.2 \times 10^{-3}$  M, linker (BDC or BPDC)  $2.2 \times 10^{-3}$  M  $\text{L}^{-1}$  and acetic acid  $420 \times 10^{-3}$  M in DMF), and then heated at  $100^\circ\text{C}$  for 3 h. After subsequent cooling down to room temperature, the obtained MOF films were dried in a vacuum.

**MOF Powder Synthesis:** The UiO-67 MOF powder was synthesized following the protocol given in the literature.<sup>[45]</sup> 53 mg of  $\text{ZrCl}_4$  (0.227 mmol) and 34 mg of 4,4-biphenyldicarboxylic acid (0.227 mmol) were mixed with 20 mL of DMF each in a Teflon-lined autoclave at room temperature. Then the mixtures were heated to  $120^\circ\text{C}$  and kept for 48 h. Following three washes with DMF, the powder was dried in air. The powder was dispersed in acetone. Finally, the powder was heated in air at  $60^\circ\text{C}$  for 12 h, then heated at  $100^\circ\text{C}$  for 1 h under reduced pressure for activation (i.e., to remove remaining acetone and DMF molecules). A MOF-ethanol emulsion (1 mg MOF per 1 mL ethanol) was drop-coated on the QCM sensor. The droplets had a volume of 40  $\mu\text{L}$  per droplet and were dried in nitrogen. The process was repeated five times.

**Uptake Experiments:** Before each uptake experiments, the samples were activated carefully in a flow of pure nitrogen at an elevated temperature ( $65^\circ\text{C}$ ) for at least 15 h. This procedure ensured that all molecules (in particular ethanol, toluene, and water) desorbed from the pores and the pores were empty before the uptake experiments. The uptake experiments were performed by instantly switching the gas flow through the QCM cell from pure nitrogen to nitrogen enriched with toluene (or the other guest molecules), using a wash bottle. This resulted in a gas flow enriched with guest-molecule vapor, where the vapor pressure was below the saturation vapor pressure at room temperature.<sup>[13,46]</sup>

**Exposure to Air:** The MOF films were exposed to the common air in the laboratory for several days. During that time, the humidity and

temperature varied between 36% and 54% as well as 22.3 and 26.7 °C, respectively.

## Supporting Information

Supporting Information is available from the Wiley Online Library or from the author.

## Acknowledgements

This research was funded by the German Research Foundation (DFG HE 7036/5) and by the China Scholarship Council (CSC).

Open access funding enabled and organized by Projekt DEAL.

## Conflict of Interest

The authors declare no conflict of interest.

## Author Contributions

The experiments and analysis of the QCM data were performed by C.L. The SEM images were recorded by A.C. and Z.Z. S.M. helped in synthesizing ZIF-8 samples. C.L. and L.H. drafted the project and wrote the manuscript.

## Data Availability Statement

The data that support the findings of this study are available from the corresponding author upon reasonable request.

## Keywords

adsorption, air exposure, degradation and stability, diffusion, metal-organic frameworks

Received: October 8, 2021

Published online:

- [1] H. Furukawa, K. E. Cordova, M. O'Keeffe, O. M. Yaghi, *Science* **2013**, *341*, 1230444.
- [2] M. Kondo, T. Yoshitomi, H. Matsuzaka, S. Kitagawa, K. Seki, *Angew. Chem., Int. Ed.* **1997**, *36*, 1725.
- [3] A. P. Côté, A. I. Benin, N. W. Ockwig, M. O'Keeffe, A. J. Matzger, O. M. Yaghi, *Science* **2005**, *310*, 1166.
- [4] A. Thomas, *Angew. Chem., Int. Ed.* **2010**, *49*, 8328.
- [5] J. R. Li, J. Sculley, H. C. Zhou, *Chem. Rev.* **2012**, *112*, 869.
- [6] Z. Gu, S. Grosjean, S. Bräse, C. Wöll, L. Heinke, *Chem. Commun.* **2015**, *51*, 8998.
- [7] S. M. Cohen, *J. Am. Chem. Soc.* **2017**, *139*, 2855.
- [8] K. Müller, J. Helfferich, F. Zhao, R. Verma, A. B. Kanj, V. Meded, D. Bléger, W. Wenzel, L. Heinke, *Adv. Mater.* **2018**, *30*, 1706551.
- [9] K. S. Park, Z. Ni, A. P. Côté, J. Y. Choi, R. Huang, F. J. Uribe-Romo, H. K. Chae, M. O'Keeffe, O. M. Yaghi, *Proc. Natl. Acad. Sci. USA* **2006**, *103*, 10186.
- [10] X. Liu, N. K. Demir, Z. Wu, K. Li, *J. Am. Chem. Soc.* **2015**, *137*, 6999.
- [11] J. A. Greathouse, M. D. Allendorf, *J. Am. Chem. Soc.* **2006**, *128*, 10678.
- [12] J. J. Low, A. I. Benin, P. Jakubczak, J. F. Abrahamian, S. A. Faheem, R. R. Willis, *J. Am. Chem. Soc.* **2009**, *131*, 15834.
- [13] L. Heinke, Z. Gu, C. Wöll, *Nat. Commun.* **2014**, *5*, 4562.
- [14] K. Müller, N. Vankova, L. Schottner, T. Heine, L. Heinke, *Chem. Sci.* **2019**, *10*, 153.
- [15] K. Vellingiri, P. Kumar, A. Deep, K.-H. Kim, *Chem. Eng. J.* **2017**, *307*, 1116.
- [16] S. Chavan, J. G. Vitillo, D. Gianolio, O. Zavorotynska, B. Civalleri, S. Jakobsen, M. H. Nilsen, L. Valenzano, C. Lamberti, K. P. Lillerud, S. Bordiga, *Phys. Chem. Chem. Phys.* **2012**, *14*, 1614.
- [17] J. B. DeCoste, G. W. Peterson, B. J. Schindler, K. L. Killops, M. A. Browe, J. J. Mahle, *J. Mater. Chem. A* **2013**, *1*, 11922.
- [18] J. Kärger, D. M. Ruthven, D. N. Theodorou, *Diffusion in Nanoporous Materials, 2 Volume Set*, John Wiley & Sons, Hoboken, NJ **2012**.
- [19] L. Heinke, P. Kortunov, D. Tzoulaki, J. Kärger, *Phys. Rev. Lett.* **2007**, *99*, 228301.
- [20] L. Heinke, J. Kärger, *New J. Phys.* **2008**, *10*, 023035.
- [21] J. C. Saint Remi, A. Lauerer, C. Chmelik, I. Vandendael, H. Terryn, G. V. Baron, J. F. Denayer, J. Kärger, *Nat. Mater.* **2016**, *15*, 401.
- [22] L. Heinke, J. Kärger, *Phys. Rev. Lett.* **2011**, *106*, 074501.
- [23] S. Liu, J. Liu, X. Hou, T. Xu, J. Tong, J. Zhang, B. Ye, B. Liu, *Langmuir* **2018**, *34*, 3654.
- [24] S. Jafari, F. Ghorbani, A. Bahrami, H. Kazemian, S. Yousefinejad, *Int. J. Sci. Stud.* **2017**, *5*, 1073.
- [25] A. Dutta, N. Tymińska, G. Zhu, J. Collins, R. P. Lively, J. R. Schmidt, S. Vasenkov, *J. Phys. Chem. C* **2018**, *122*, 7278.
- [26] J. Kärger, *Microporous Mesoporous Mater.* **2014**, *189*, 126.
- [27] R. Wang, B. C. Bukowski, J. Duan, T. R. Sheridan, A. Atilgan, K. Zhang, R. Q. Snurr, J. T. Hupp, *Langmuir* **2020**, *36*, 10853.
- [28] M. Jahandar Lashaki, M. Fayaz, S. Niknaddaf, Z. Hashisho, *J. Hazard. Mater.* **2012**, *241–242*, 154.
- [29] Y. Hu, H. Kazemian, S. Rohani, Y. Huang, Y. Song, *Chem. Commun.* **2011**, *47*, 12694.
- [30] S. Jafari, F. Ghorbani-Shahna, A. Bahrami, H. Kazemian, *Appl. Sci.* **2018**, *8*, 310.
- [31] X. Liu, H. Jin, Y. Li, H. Bux, Z. Hu, Y. Ban, W. Yang, *J. Membr. Sci.* **2013**, *428*, 498.
- [32] S. Tanaka, Y. Tanaka, *ACS Omega* **2019**, *4*, 19905.
- [33] Y. Han, M. Liu, K. Li, Y. Zuo, Y. Wei, S. Xu, G. Zhang, C. Song, Z. Zhang, X. Guo, *CrystEngComm* **2015**, *17*, 6434.
- [34] L. Valenzano, B. Civalleri, S. Chavan, S. Bordiga, M. H. Nilsen, S. Jakobsen, K. P. Lillerud, C. Lamberti, *Chem. Mater.* **2011**, *23*, 1700.
- [35] J. B. Decoste, G. W. Peterson, M. W. Smith, C. A. Stone, C. R. Willis, *J. Am. Chem. Soc.* **2012**, *134*, 1486.
- [36] Y.-J. Lee, Y.-J. Chang, D.-J. Lee, J.-P. Hsu, *J. Taiwan Inst. Chem. Eng.* **2018**, *93*, 176.
- [37] A. Pankajakshan, M. Sinha, A. A. Ojha, S. Mandal, *ACS Omega* **2018**, *3*, 7832.
- [38] J. B. DeCoste, G. W. Peterson, H. Jasuja, T. G. Glover, Y.-g. Huang, K. S. Walton, *J. Mater. Chem. A* **2013**, *1*, 5642.
- [39] N. C. Burtch, H. Jasuja, K. S. Walton, *Chem. Rev.* **2014**, *114*, 10575.
- [40] M. C. Lawrence, C. Schneider, M. J. Katz, *Chem. Commun.* **2016**, *52*, 4971.
- [41] G. Ayoub, T. Islamoglu, S. Goswami, T. Friščić, O. K. Farha, *ACS Appl. Mater. Interfaces* **2019**, *11*, 15788.
- [42] K. Wang, H. Huang, X. Zhou, Q. Wang, G. Li, H. Shen, Y. She, C. Zhong, *Inorg. Chem.* **2019**, *58*, 5725.
- [43] E. P. Valadez Sánchez, H. Gliemann, K. Haas-Santo, C. Wöll, R. Dittmeyer, *Chem. Ing. Tech.* **2016**, *88*, 1798.
- [44] E. Virmani, J. M. Rotter, A. Mähringer, T. von Zons, A. Godt, T. Bein, S. Wuttke, D. D. Medina, *J. Am. Chem. Soc.* **2018**, *140*, 4812.
- [45] J. H. Cavka, S. Jakobsen, U. Olsbye, N. Guillou, C. Lamberti, S. Bordiga, K. P. Lillerud, *J. Am. Chem. Soc.* **2008**, *130*, 13850.
- [46] L. Heinke, *J. Phys. D: Appl. Phys.* **2017**, *50*, 193004.